Modeling Gas Solubilities in the Aqueous Solution of Methyldiethanolamine

ARTICLE *in* INDUSTRIAL & ENGINEERING CHEMISTRY RESEARCH · APRIL 2011

Impact Factor: 2.59 · DOI: 10.1021/ie102150h

2 AUTHORS:

Ying Zhang
Aspen Technology, Inc.
5 PUBLICATIONS **178** CITATIONS
SEE PROFILE

Chau-Chyun Chen
Texas Tech University
93 PUBLICATIONS **3,384** CITATIONS
SEE PROFILE

I&EC research
Industrial & Engineering Chemistry Research

ARTICLE

pubs.acs.org/IECR

Modeling Gas Solubilities in the Aqueous Solution of Methyldiethanolamine

Ying Zhang[†] and Chau-Chyun Chen[‡,*]

[†]AspenTech Limited, Pudong, Shanghai 201203, China

[‡]Aspen Technology, Inc. Burlington, Massachusetts 01803, United States

ABSTRACT: A thermodynamically consistent model recently developed for representing CO_2 solubility in aqueous solutions of methyldiethanolamine is extended to include H_2S and lower hydrocarbons. The electrolyte−nonrandom two-liquid (NRTL) activity coefficient model and the PC-SAFT equation of state are used to represent the liquid phase and the vapor phase nonideality, respectively. The Henry's constant of H_2S in water is fitted to the total pressure data of the H_2S-H_2O binary system. The NRTL binary interaction parameters of the solvent−electrolyte binaries are regressed with the VLE data of the H_2S-H_2O-MDEA ternary system. The differential heat of H_2S absorption of the H_2S-H_2O-MDEA ternary system and the partial pressures of H_2S and CO_2 of the $H_2S-CO_2-H_2O-$MDEA quaternary system are predicted and compared favorably to the experimental data. The Henry's constants of light hydrocarbons in water and MDEA are also determined by fitting the total pressure data of the hydrocarbon−H_2O binary and the hydrocarbon−H_2O-MDEA ternary systems.

1. INTRODUCTION

Aqueous methyldiethanolamine (MDEA) solutions are widely used in the natural gas industry to strip acid gases (CO_2 and H_2S) from natural gas. Design of gas treating processes with aqueous MDEA solutions requires accurate vapor−liquid equilibrium (VLE) and enthalpy calculations for the acid gas−H_2O-MDEA system. Solubilities of light hydrocarbons in aqueous MDEA solutions are also important as they determine the magnitude of loss of hydrocarbon in the gas treating process. In this work, we extend our recent modeling work on the CO_2-H_2O-MDEA system[1] to H_2S and hydrocarbons in aqueous MDEA solutions. This extended model should provide accurate VLE and enthalpy calculations for process modeling and simulation of natural gas treating processes with aqueous MDEA solutions.

2. THERMODYNAMIC MODEL

The acid gas solubility in aqueous amine solutions is determined by both its physical solubility and the chemical equilibrium of the aqueous phase ionic reactions among the acid gases, water, and amines.

In aqueous solutions, acid gases H_2S and CO_2 react with MDEA. The ionic equilibrium reactions are expressed as

$$2H_2O \leftrightarrow H_3O^+ + OH^- \quad (1)$$

$$MDEAH^+ + H_2O \leftrightarrow H_3O^+ + MDEA \quad (2)$$

$$H_2S + H_2O \leftrightarrow H_3O^+ + HS^- \quad (3)$$

$$HS^- + H_2O \leftrightarrow H_3O^+ + S^{-2} \quad (4)$$

$$CO_2 + 2H_2O \leftrightarrow H_3O^+ + HCO_3^- \quad (5)$$

Table 1. Parameters for the PC-SAFT Equation of State[a]

	m	ε (K)	σ (Å)	ε^{AB} (K)	k^{AB} (Å^3)	source
H_2S	1.6631	229.3	3.0404	0	0	Aspen databank[7]
H_2O	1.0656	366.51	3.0007	2500.7	0.034868	Gross and Sadowski[6]
MDEA	3.3044	237.44	3.5975	3709.9	0.066454	Zhang and Chen[1]
CO_2	2.5692	152.10	2.5637	0	0	Aspen databank[7]
CH_4	1.0	150.03	3.7039	0	0	Aspen databank[7]
C_2H_6	1.6069	191.42	3.5206	0	0	Aspen databank[7]
C_3H_8	2.0020	208.11	3.6184	0	0	Aspen databank[7]
C_4H_{10}	2.3316	222.88	3.7086	0	0	Aspen databank[7]

[a] Definitions: m, segment number parameter; ε, segment energy parameter; σ, segment size parameter; ε^{AB}, association energy parameter; k^{AB}, effective association volume parameter.

$$HCO_3^- + H_2O \leftrightarrow H_3O^+ + CO_3^{-2} \quad (6)$$

The liquid phase compositions must satisfy the chemical equilibrium relationships:

$$K_j = \frac{\prod_{i'} (x_{i'}\gamma_{i'})^{\nu_{i'}}}{\prod_i (x_i\gamma_i)^{\nu_i}} \quad (7)$$

where K_j is the chemical equilibrium constant of reaction j; x_i is the mole fraction of reactant component i in reaction j; $x_{i'}$ is the mole fraction of product component i' in reaction j; γ_i and $\gamma_{i'}$ are the symmetric activity coefficients of solvents, that is, water and amines,

Received: October 23, 2010
Accepted: March 30, 2011
Revised: March 24, 2011

   dx.doi.org/10.1021/ie102150h | Ind. Eng. Chem. Res. XXXX, XXX, 000–000

Table 2. Summary of Model Parameters for the $H_2S-H_2O-MDEA$ System

parameters	component	source
Antoine equation parameter	MDEA	Zhang and Chen[1]
heat of vaporization, $\Delta_{vap}H$	MDEA	Zhang and Chen[1]
dielectric constant, ε	MDEA	Aspen Databank[7]
ideal gas Gibbs energy of formation at 298.15 K, $\Delta_f G^{ig}_{298.15}$	H_2O, MDEA, H_2S	Aspen Databank[7]
ideal gas enthalpy of formation at 298.15 K, $\Delta_f H^{ig}_{298.15}$	H_2O, MDEA, H_2S	Aspen Databank[7]
ideal gas heat capacity, C_p^{ig}	H_2O, H_2S	Aspen Databank[7]
	MDEA	Zhang and Chen[1]
molality scale Gibbs energy of formation in aqueous phase infinite dilution at 298.15 K, $\Delta_f G^{\infty,aq}_{298.15}$	H_3O^+, OH^-, HS^-, S^{-2}	Aspen Databank[7] and Wagman et al.[8]
	$MDEAH^+$	Zhang and Chen[1]
enthalpy of formation in aqueous phase infinite dilution at 298.15 K, $\Delta_f H^{\infty,aq}_{298.15}$	H_3O^+, OH^-, HS^-, S^{-2}	Aspen Databank[7] and Wagman et al.[8]
	$MDEAH^+$	Zhang and Chen[1]
heat capacity in aqueous phase infinite dilution, $C_p^{\infty,aq}$	H_3O^+, OH^-	Aspen Databank[7]
	HS^-, S^{-2}	Criss and Cobble[9]
	$MDEAH^+$	Zhang and Chen[1]
PC-SAFT parameters, m, ε, σ, ε^{AB}, k^{AB} for the pure component and $k^{ij}$for binary	H_2O	Gross and Sadowski[6]
	MDEA	Zhang and Chen[1]
	H_2S	Aspen databank[7]
	$H_2O-MDEA$ binary, H_2S-H_2O binary, H_2S-MDEA binary	set to zero
Henry's constant parameter	H_2S in H_2O	regression[a]
	H_2S in MDEA	this work
Brelvi–O'Connell characteristic volume, V^{BO}	H_2O, MDEA, H_2S,	Aspen databank[7]
NRTL binary parameters	H_2S-H_2O binary	set to zero
	MDEA-H_2O binary	Zhang and Chen[1]
	H_2O-($MDEAH^+$, HS^-) binary, MDEA-($MDEAH^+$, HS^-) binary	regression[b]

[a] Data used for regression: VLE data of H_2S-H_2O binary. [b] Data used for regression: VLE data of $H_2S-H_2O-MDEA$ ternary.

Table 3. Parameters for Reference State Properties (in J $kmol^{-1}$)

property	$\Delta_f G^{ig}_{298.15}$	$\Delta_f H^{ig}_{298.15}$	$\Delta_f G^{\infty,aq}_{298.15}$	$\Delta_f H^{\infty,aq}_{298.15}$	source
H_2S	-3.3440×10^7	-2.0630×10^7			Aspen Databank[7]
H_2O	-2.2859×10^8	-2.4181×10^8			Aspen Databank[7]
MDEA	-1.6900×10^8	-3.8000×10^8			Aspen Databank[7]
CO_2	-3.9437×10^8	-3.9351×10^8			Aspen Databank[7]
HS^-			1.2080×10^7	-1.7600×10^7	Wagman et al.[8]
S^{-2}			8.5800×10^7	3.3100×10^7	Wagman et al.[8]
H_3O^+			-2.3713×10^8	-2.8583×10^8	Aspen Databank[7]
OH^-			-1.5724×10^8	-2.2999×10^8	Wagman et al.[8]
$MDEAH^+$			-2.5952×10^8	-5.1095×10^8	Zhang and Chen[1]
HCO_3^-			-5.8677×10^8	-6.9199×10^8	Wagman et al.[8]
CO_3^{-2}			-5.2781×10^8	-6.7714×10^8	Wagman et al.[8]

Table 4. Antoine Equation Parameters for Pure MDEA[a]

	C_{1i}	C_{2i}	C_{3i}	C_{4i}	source
MDEA	1.2276×10^2	-1.3253×10^4	-1.3839×10^1	3.20×10^{-6}	Aspen Databank[7]

[a] Correlation for Antoine equation, $\ln(P_i^*,l/Pa) = C_{1i} + (C_{2i})/(T\,(K)) + C_{3i}\ln(T\,(K)) + C_{4i}(T\,(K))^2$.

and the unsymmetric activity coefficients of molecular or ionic solutes i and i' in aqueous solution and are normalized to the aqueous phase infinite dilution reference state; and ν_i and $\nu_{i'}$ are the stoichiometric coefficients of reactants and products, respectively.

dx.doi.org/10.1021/ie102150h |*Ind. Eng. Chem. Res.* XXXX, XXX, 000–000

Chemical equilibrium constants for the ionic reactions can be calculated from the reference state Gibbs energies of the participating species:

$$-RT \ln K_j = \Delta G_j^\circ(T) \quad (8)$$

where $\Delta G_j^\circ(T)$ is the reference state Gibbs energy change for reaction j at temperature T, R is the universal gas constant, and T is the system temperature.

Table 5. Parameters for Heat of Vaporization[a]

	C_{1i}	C_{2i}	T_{ci}	source
MDEA	9.7381×10^7	4.6391×10^{-1}	741.9	Aspen Databank[7]

[a] DIPPR equation for heat of vaporization, $\Delta_{vap}H_i$/J kmol^{-1} = $C_{1i}(1 - T_{ri})^{C_{2i}}$, $T_{ri} = (T\ (\mathrm{K}))/(T_{ci}\ (\mathrm{K}))$, T_{ci} is critical temperature of component i.

Table 6. Parameters for Dielectric Constant[a]

	A_i	B_i	C_i	source
MDEA	21.9957	8992.68	298.15	Aspen Databank[7]

[a] Correlation for dielectric constant, $\varepsilon_i = A_i + B_i(1/(T\ (\mathrm{K})) - 1/(C_i))$

Table 7. Parameters for Henry's constant[a]

solute i	solvent j	a_{ij}	b_{ij}	c_{ij}	d_{ij}	source
H_2S	H_2O	151.031	−6415.26	−20.3806	0.01476	this work
H_2S	MDEA	151.031	−6415.26	−20.3806	0.01476	this work[b]
CO_2	H_2O	100.65	−6147.7	−10.191	−0.010	Yan and Chen[10]
CO_2	MDEA	19.8933	−1072.7	0.0	0.0	Zhang and Chen[1]
CH_4	H_2O	188.529	−8720.4	−24.072	0	this work
CH_4	MDEA	−19.586	−2401.0	−5.765	0	this work
C_2H_6	H_2O	247.809	−11988.3	−32.592	0	this work
C_2H_6	MDEA	−23.905	2435.5	6.111	0	this work
C_3H_8	H_2O	350.878	−17129.0	−47.638	0	this work
C_3H_8	MDEA	−216.864	12221.1	34.167	0	this work
C_4H_{10}	H_2O	898.953	−44053.7	−127.985	0	this work
C_4H_{10}	MDEA	−345.518	20003.5	52.064	0	this work

[a] Correlation for Henry's constant, $\ln(H_{ij}/P_a) = a_{ij} + b_{ij}/(T\ (\mathrm{K})) + c_{ij}\ln(T\ (\mathrm{K})) + d_{ij}(T\ (\mathrm{K}))$. [b] Henry's constant of H_2S in MDEA is set to be same as that of H_2S in water.

Table 8. Parameters for Ideal Gas Heat Capacity (in J kmol^{-1}·K^{-1})[a]

	H_2S[b]	MDEA	H_2O	CO_2
source	Aspen Databank[7]	Zhang and Chen[1]	Aspen Databank[7]	Aspen Databank[7]
C_{1i}	3.3288×10^4	2.7303×10^4	3.3738×10^4	1.9795×10^4
C_{2i}	2.6086×10^4	5.4087×10^2	−7.0176	7.3437×10^1
C_{3i}	9.134×10^2	0	2.7296×10^{-2}	-5.6019×10^{-2}
C_{4i}	-1.7979×10^4	0	-1.6647×10^{-5}	1.7153×10^{-5}
C_{5i}	9.494×10^2	0	4.2976×10^{-9}	0
C_{6i}	0	0	-4.1696×10^{-13}	0
C_{7i}	100	278	200	300
C_{8i}	1500	397	3000	1088.6

[a] Correlation for ideal gas heat capacity, C_p^{ig}/J kmol^{-1} K^{-1} = $C_{1i} + C_{2i}(T\ (\mathrm{K})) + C_{3i}(T\ (\mathrm{K}))^2 + C_{4i}(T\ (\mathrm{K}))^3 + C_{5i}(T\ (\mathrm{K}))^4 + C_{6i}(T\ (\mathrm{K}))^5$, $C_{7i} < T < C_{8i}$. [b] Correlation for ideal gas heat capacity of H_2S, C_p^{ig}/J kmol^{-1} K^{-1} = $C_{1i} + C_{2i}((C_{3i}/(T\ (\mathrm{K})))/(\sinh(C_{3i}/(T\ (\mathrm{K})))))^2 + C_{4i}((C_{5i}/(T\ (\mathrm{K})))/(\cosh(C_{5i}/(T\ (\mathrm{K})))))^2$, $C_{7i} < T < C_{8i}$

Table 9. Parameters for Aqueous Phase Infinite Dilution Heat Capacity[a]

	C_1	Source
HS^-	-1.5884×10^5[b]	this work
S^{-2}	-4.0061×10^4[b]	this work
H_3O^+	7.5291×10^4	Aspen Databank[7]
OH^-	-1.4845×10^5	Aspen Databank[7]
$MDEAH^+$	3.3206×10^5	Zhang and Chen[1]
HCO_3^-	-2.9260×10^4	Zhang and Chen[1]
CO_3^{-2}	-3.9710×10^5	Zhang and Chen[1]

[a] Correlation for aqueous phase infinite dilution heat capacity, $C_{p,i}^{\infty,aq}$/J kmol^{-1} K^{-1} = C_1. [b] $C_{p,i}^{\infty,aq}$ value of HS^- is the average value of heat capacity between 298 and 473 K taken from Criss and Cobble (1968),[9] and that of S^{-2} is calculated from the Criss−Cobble correlation[9] with the entropy value from Wagman et al. (1982).[8]

Table 10. Parameters of the Characteristic Volume (in m^3 kmol^{-1}) for the Brelvi−O'Connell Model[a]

	v_1	v_2	source
H_2S	0.0985	0	Aspen Databank[7]
H_2O	0.464	0	Aspen Databank[7]
MDEA	0.369	0	Aspen Databank[7]
CO_2	0.177	-3.42×10^{-4}	Yan and Chen[10]
CH_4	0.0736	0	this work
C_2H_6	0.1393	0	this work
C_3H_8	0.2000	0	Aspen Databank[7]
C_4H_{10}	0.2550	0	Aspen Databank[7]

[a] Correlation for the characteristic volume parameters, V_i^{BO} (m^3 kmol^{-1}) = $v_1 + v_2(T\ (\mathrm{K}))$.

Table 11. NRTL parameters τ_{ij}[a] for MDEA-H_2O Binary with α = 0.2

parameter	component i	component j	value	source
a_{ij}	H_2O	MDEA	8.5092	Zhang and Chen[1]
a_{ij}	MDEA	H_2O	−1.7141	
b_{ij}	H_2O	MDEA	−1573.9	
b_{ij}	MDEA	H_2O	−261.85	

[a] Correlation for the NRTL parameters, $\tau_{ij} = a_{ij} + b_{ij}/(T/\mathrm{K})$

Table 12. NRTL Parameters τ_{ij} for Molecule−Electrolyte Binaries with α = 0.2

component i	component j	value	source
H_2O	($MDEAH^+$, HCO_3^-)	8.7170	Zhang and Chen[1]
($MDEAH^+$, HCO_3^-)	H_2O	−4.2995	
H_2O	($MDEAH^+$, CO_3^{-2})	10.4032	
($MDEAH^+$, CO_3^{-2})	H_2O	−4.9252	
MDEA	($MDEAH^+$, HCO_3^-)	5.2964	
($MDEAH^+$, HCO_3^-)	MDEA	−0.8253	
H_2O	($MDEAH^+$, HS^-)	4.0564	this work
($MDEAH^+$, HS^-)	H_2O	−1.7522	
MDEA	($MDEAH^+$, HS^-)	7.4499	
($MDEAH^+$, HS^-)	MDEA	−1.9446	

dx.doi.org/10.1021/ie102150h |Ind. Eng. Chem. Res. XXXX, XXX, 000–000

Table 13. Experimental Data Used in the Regression for the H_2S-H_2O System

data type	T (K)	P (kPa)	H_2S mole fraction	data points	average relative deviation, $\lvert\Delta P/P\rvert$ (%)	reference
VLE, *TPx*, total pressure	278−333	37−494	0.0006−0.007	34	7.1	Wright and Maass[11]
VLE, *TPx*, total pressure	303−316	1720	0.019−0.025	15	5.4	Pohl[12]
VLE, *TPx*, total pressure	303−443	1720−2340	0.005−0.03	39	9.8	Burgess and Germann[13]
VLE, *TPx*, total pressure	273−323	47−96	0.0005−0.003	36	5.8	Clarke and Glew[14]
VLE, *TPx*, total pressure	283−453	155−6670	0.0003−0.037	325	5.5	Lee and Mather[15]
VLE, *TPx*, total pressure	311−478	345−10300	0.004−0.041	12	7.6	Gillespie and Wilson[16]
VLE, *TPx*, total pressure	294−594	222−13900	0.002−0.016	49	10.5	Suleimenov and Krupp[17]
VLE, *TPx*, total pressure	313	470−2490	0.006−0.03	9	4.2	Kuranov et al.[18]

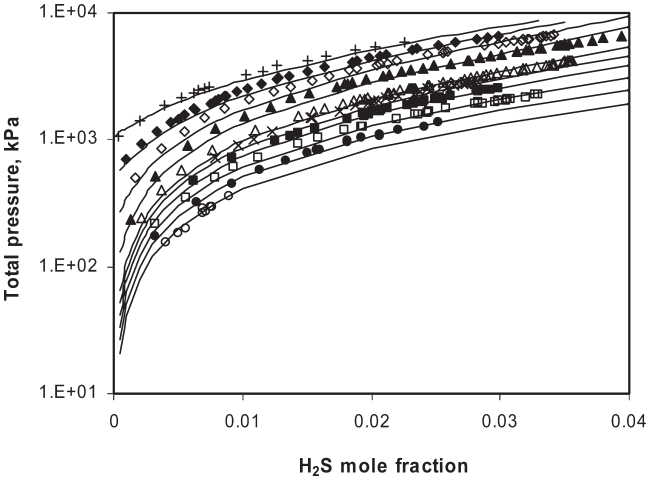

Figure 1. Comparison of the experimental data from Lee and Mather[15] (symbols) for total pressure of binary H_2S-H_2O solution and the model results (lines): (○) T = 283, (●) T = 293, (□) T = 303, (■) T = 313, (×) T = 323, (△) T = 333, (▲) T = 363, (◇) T = 393, (◆) T = 423, (+) T = 453 K.

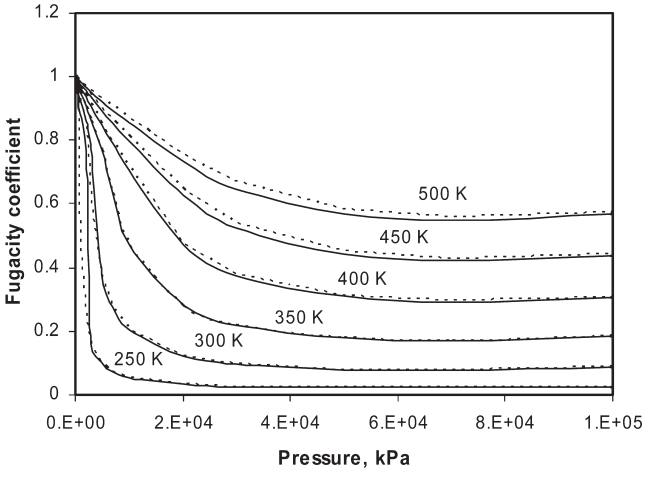

Figure 2. Vapor phase fugacity coefficient for pure H_2S: (solid line) PC-SAFT results, (dotted line) GERG2008 results.

The physical solubility of the acid gas is calculated from Henry's law:

$$P \cdot y_i \cdot \phi_i = H_i \cdot x_i \cdot \gamma_i^* \qquad (9)$$

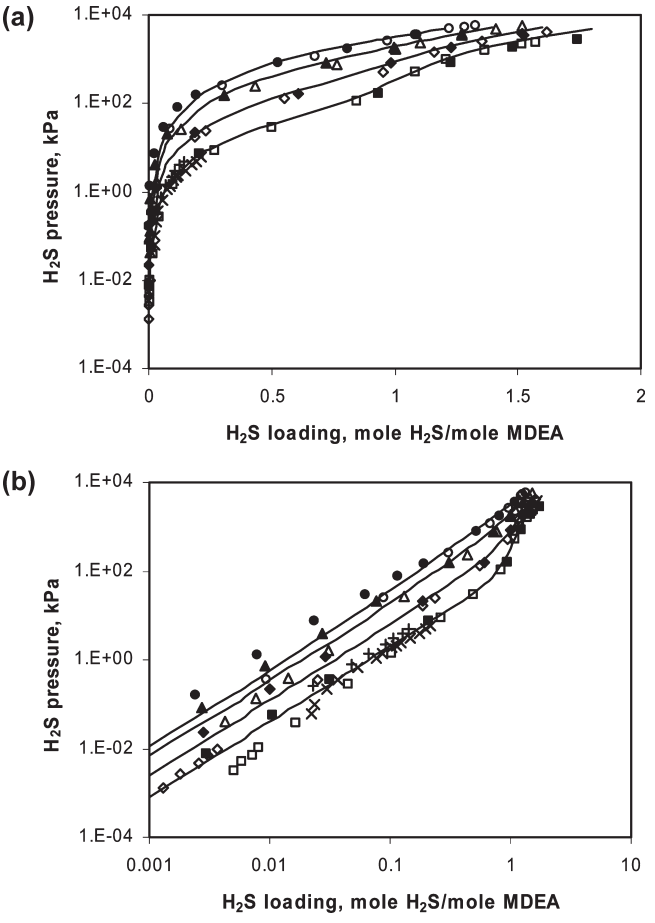

Figure 3. Comparison of the experimental data (symbols) and the model results (lines) for H_2S partial pressure of H_2S-H_2O-MDEA solution. MDEA mole fraction is 0.13. The empty symbols represent the experimental data from Jou et al.:[20] (□) T = 313, (◇), T = 343, (△)T = 373, (○) T = 393 K, the full symbols represent the experimental data from Huang and Ng,[26] (■), T = 313, (◆) T = 343, (▲) T = 373, (●) T = 393 K; (×) experimental data of Jou et al.[24] at 313 K; (+) experimental data of ter Maat et al.[22] at 313 K.

where P is the system pressure, y_i is the mole fraction of component i in the vapor phase, ϕ_i is the fugacity coefficient of component i in the vapor phase, H_i is the Henry's law constant of component i in the mixed solvent of water and amine, x_i is the equilibrium mole fraction of component i in the liquid phase, and γ_i^* is the unsymmetric activity coefficient of component i in the mixed solvent solution of water and amine

dx.doi.org/10.1021/ie102150h |*Ind. Eng. Chem. Res.* XXXX, XXX, 000–000

Table 14. Experimental Data Used in the Regression for the $H_2S-H_2O-MDEA$ System

data type	T (K)	P (kPa)	MDEA mole fraction	H_2S loading	data points	average relative deviation, $\lvert\Delta P/P\rvert$ (%)	reference
VLE, *TPx*, H_2S pressure	298−393	0.13−5900	0.02−0.13	0.0076−3.2	108	31.9	Jou et al.[20]
VLE, *TPx*, H_2S pressure	298−389	13−1500	0.02−0.036	0.18−2.17	49	13.0	Maddox et al.[21]
VLE, *TPx*, H_2S pressure	283−313	0.14−19	0.075−0.131	0.02−0.57	37	29.5	ter Maat et al.[22]

Table 15. Comparison between Experimental Data and Model Predictions for Total Pressure or H_2S Partial Pressure of the $H_2S-H_2O-MDEA$ System

data type	*T* (K)	*P* (kPa)	MDEA mole fraction	H_2S loading	data points	average relative deviation, $\lvert\Delta P/P\rvert$ (%)	reference
VLE, *TPx*, H_2S pressure	313	0.5−1600	0.045	0.13−1.73	27	64.7	Macgregor and Mather[23]
VLE, *TPx*, H_2S pressure	313−373	0.002−310	0.075−0.13	0.004−1.08	50	34.5	Jou et al.[24]
VLE, *TPx*, H_2S pressure	313−373	1.5−450	0.062	0.08−0.90	43	45.1	Li and Shen[25]
VLE, *TPx*, total pressure	313−413	170−4900	0.034−0.067	0.48−1.93	71	9.4	Kuranov et al.[18]
VLE, *TPx*, H_2S pressure	298−393	0.0013−5900	0.02−0.13	0.0013−3.2	150	27.9	Huang and Ng[26]
VLE, *TPx*, H_2S pressure	298−313	0.03−1.6	0.020−0.045	0.01−0.26	29	30.4	Lemoine et al.[27]
VLE, *TPx*, total pressure	313−393	200−6000	0.126	0.15−1.43	26	12.4	Pèrez-Salado Kamps et al.[28]
VLE, *TPx*, total pressure	313−373	6−1000	0.117	0−0.12	27	12.1	Sidi-Boumedine et al.[29]

and is normalized to the mixed solvent infinite dilution reference state.

The Henry's law constant in the mixed solvent can be calculated from those in the pure solvents:[1]

$$\ln\left(\frac{H_i}{\gamma_i^{\infty}}\right) = \sum_A w_A \ln\left(\frac{H_{iA}}{\gamma_{iA}^{\infty}}\right) \tag{10}$$

where H_i is the Henry's constant of molecular solute i in the mixed solvent, H_{iA} is the Henry's constant of solute i in pure solvent A, γ_i^{∞} is the infinite dilution activity coefficient of solute i in the mixed solvent, γ_{iA}^{∞} is the infinite dilution activity coefficient of solute i in pure solvent A, and w_A is a weighting factor calculated by eq 11:

$$w_A = \frac{x_A\left(V_{iA}^{\infty}\right)^{2/3}}{\sum_B x_B\left(V_{iB}^{\infty}\right)^{2/3}} \tag{11}$$

where V_{iA}^{∞} is the partial molar volume of solute i at infinite dilution in pure solvent A, and is calculated from the Brelvi−O'Connell model[2] with the characteristic volume for the solute (V_i^{BO}) and solvent (V_s^{BO}).

The Henry's constant of solute i in solvent A is further corrected with the Poynting term for pressure:

$$H_{iA}(T,P) = H_{iA}(T,p_A^{\circ,l}) \exp\left(\frac{1}{RT}\int_{p_A^{\circ,l}}^{P} V_{iA}^{\infty}\, dp\right) \tag{12}$$

where $H_{iA}(T,P)$ is the Henry's constant of solute i in solvent A at system temperature and pressure, $H_{iA}(T,p_A^{o,l})$ is the Henry's constant of solute i in solvent A at system temperature and the solvent vapor pressure, and V_{iA}^{∞} is the partial molar volume of solute i at infinite dilution in solvent A calculated from the Brelvi−O'Connell model.

The detailed thermodynamic model for the $CO_2-H_2O-MDEA$ system has been presented in an earlier work.[1] We do not repeat the equations for the thermodynamic framework in this paper. The 2009 version of the electrolyte−nonrandom two-liquid (NRTL) model[3,4] is used to calculate activity coefficients required in the aqueous phase chemical equilibrium calculations and the mixed solvent phase equilibrium calculations. Unless specified otherwise, all molecule−molecule binary parameters and electrolyte−electrolyte binary parameters are defaulted to zero, and all molecule−electrolyte binary parameters are defaulted to (8, −4), the average values of the parameters as reported for the electrolyte NRTL model.[4] The nonrandomness factor, α, is fixed at 0.2.

The PC-SAFT[5,6] equation of state (EOS) is used to calculate the vapor phase fugacity coefficients. Reported in Table 1, the PC-SAFT EOS pure component parameters are taken from our earlier work for the $CO_2-H_2O-MDEA$ system,[1] Gross and Sadowski (2002),[6] and the Aspen Plus databank.[7] The binary PC-SAFT interaction parameters are all set to 0.

Table 2 summarizes the model parameters and the sources of the parameters used in the $H_2S-H_2O-MDEA$ thermodynamic model. The model parameters include pure component parameters and thermodynamic constants for the molecular and ionic species, PC-SAFT EOS parameters, Henry's constant and Brelvi−O'Connell characteristic volume parameters, and binary interaction parameters associated with the electrolyte NRTL model. Most of the parameters can be obtained from our earlier work[1] and the literature;[6−9] the remaining parameters are determined by fitting to the experimental data. Note that while the model parameters and the sources of the parameters used in the $CO_2-H_2O-MDEA$ model have been summarized in our previous work,[1,10] we present in this work all the model parameters required for modeling the solubilities of CO_2, H_2S, and light hydrocarbons in aqueous MDEA solution for completeness. In addition to the PC-SAFT parameters reported in Table 1, values of the remaining parameters are summarized in Tables 3−12.

dx.doi.org/10.1021/ie102150h |*Ind. Eng. Chem. Res.* XXXX, XXX, 000–000

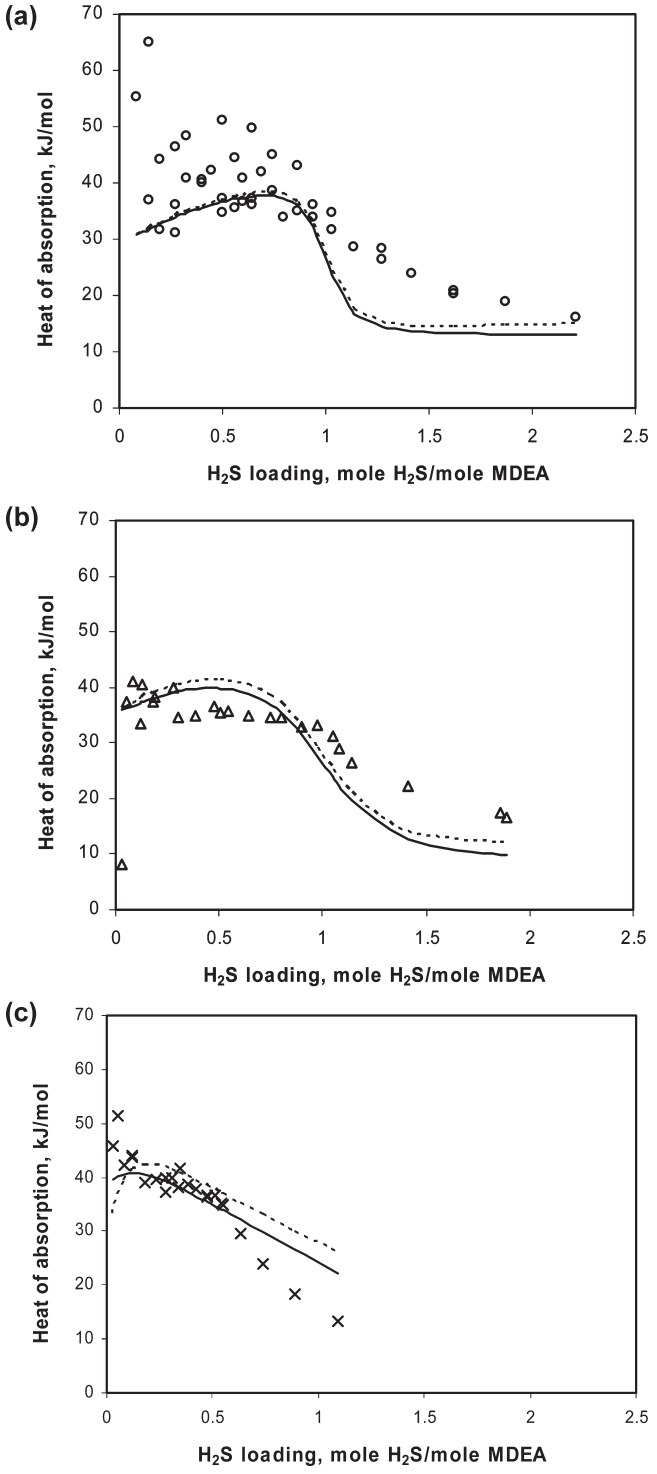

Figure 4. Comparison of the experimental data from Oscarson and Izatt[31] (symbols) and the model results (lines) for differential heat of H_2S absorption in aqueous MDEA solution. MDEA mole fraction is 0.13. (○) T = 300, (△) T = 350, (×) T = 400 K; (solid line) prediction according to enthalpy balance; (dotted line) prediction according to Gibbs−Helmholtz equation.

3. MODELING RESULTS

We first extend the thermodynamic model for the CO_2−H_2O−MDEA system to cover the H_2S−H_2O−MDEA system. We then predict the partial pressures of the acid gases for the H_2S-CO_2−H_2O−MDEA system based on the CO_2−H_2O−MDEA and H_2S−H_2O−MDEA models. For the hydrocarbon−H_2O−MDEA system, we consider their physical solubility and fit the VLE data with the Henry's constants.

3.1. H_2S−H_2O System. Summarized in Table 13 are the extensive experimental total pressure data available for the H_2S−H_2O system.[11−18] These data cover temperature from 273 to 594 K and pressure from 37 to 13900 kPa. We use these data in the regression to determine the Henry's constant of H_2S in water. Also given in Table 13 are the excellent correlation results with average relative deviations of less than 10% for all data sets. As an example, Figure 1 shows that the total pressure data of Lee and Mather (1977)[15] for the H_2S−H_2O binary are represented well. The regressed parameters for the Henry's constant are given in Table 7.

To check reliability of the model predictions for H_2S solubility above 13900 kPa, we show in Figure 2 the vapor fugacity coefficients of pure H_2S calculated with the PC-SAFT EOS up to 100000 kPa and those calculated with the GERG2008 EOS.[19] As the GERG2008 EOS provides a high fidelity representation of the H_2S PVT data, the satisfactory match between the results of the PC-SAFT EOS and those from the GERG2008 EOS suggests the extrapolation of H_2S fugacity to high pressure with PC-SAFT is reliable.

3.2. H_2S−H_2O−MDEA System. Extensive VLE data are available for the H_2S−H_2O−MDEA ternary system.[18,20−29] We select the data of Jou et al. (1982),[20] Maddox et al. (1987),[21] and ter Maat et al. (2004)[22] to minimize the impact of data inconsistency and to cover the wide ranges for temperature from 283 to 393 K, pressure from 0.13 to 5900 kPa, MDEA mole fraction from 0.02 to 0.13, and H_2S loading from 0.0076 to 3.2. The remaining literature data are used for model validation only.

Figure 3 panels a and b show that, as the H_2S loading decreases, scattering on the reported H_2S partial pressures increases. The Jou et al.[20] data deviate from the others[22,24,26] especially at low pressures. Therefore, the data set of Jou et al.[20] is limited to the data with H_2S pressure above 0.1 kPa in the regression. The VLE data of Huang and Ng (1998)[26] also cover wide ranges for temperature, pressure, MDEA concentration, and H_2S loading. However, as shown in Figure 3, panels a and b, the high temperature data of Huang and Ng[26] are found to be severely inconsistent with those from Jou et al.[20] Specifically, the H_2S partial pressures at temperatures of 373K and 393K reported by Huang and Ng[26] are almost 1 order of magnitude higher than those reported by Jou et al.[20] We further find that the VLE predictions for the H_2S-CO_2−H_2O−MDEA quaternary system are highly sensitive to whether Huang and Ng's data[26] are used in the regression of the molecule-electrolyte NRTL binary parameters. Specifically, the VLE predictions from the model for the H_2S-CO_2−H_2O−MDEA system show strong deviations from the experimental data[22,25,30] when Huang and Ng's VLE data for the H_2S−H_2O−MDEA system are included in the regression. Therefore the VLE data of Huang and Ng[26] are not used in regression.

The selected experimental data are correlated with the model by adjusting the four NRTL binary interaction parameters for the two major molecule−electrolyte binaries, that is, the H_2O−($MDEAH^+$, HS^-) binary and the MDEA−($MDEAH^+$, HS^-)

Table 16. Comparison between Experimental Data and Model Predictions for H_2S Partial Pressure and CO_2 Partial Pressure of the $H_2S-CO_2-H_2O-$MDEA System

data type	VLE, *TPx*, partial pressures	VLE, *TPx*, partial pressures	VLE, *TPx*, partial pressures
T (K)	283−298	311−373	323
P (kPa), H_2S pressure	0.12−35	0.38−65	6−680
P (kPa), CO_2 pressure	0.08−15	0.14−770	10−1150
MDEA mole fraction	0.075−0.13	0.13	0.13
H_2S loading	0.02−0.59	0.01−0.30	0.11−0.88
CO_2 loading	0.05−0.40	0.002−0.64	0.09−0.71
data points	73	16	18
average relative deviation of H_2S partial pressure, $\lvert\Delta P/P\rvert$, %	26.2	49.5	25.1
average relative deviation of CO_2 partial pressure, $\lvert\Delta P/P\rvert$, %	37.3	66.6	42.5
reference	ter Maat et al.[22]	Huang and Ng[26]	Dicko et al.[30]

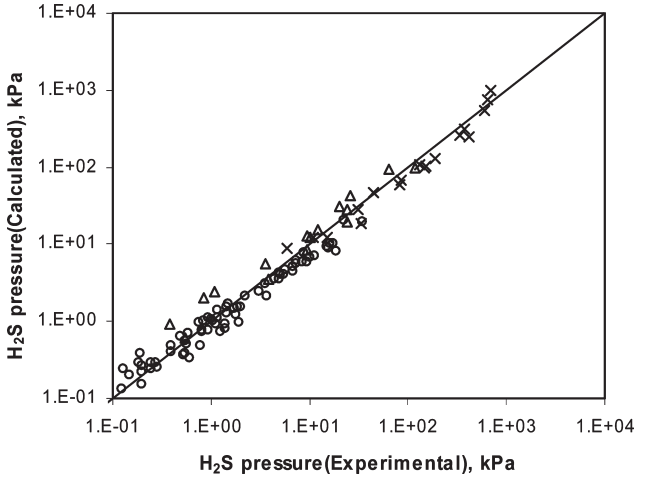

Figure 5. Parity plot for H_2S partial pressure of $H_2S-CO_2-H_2O-$MDEA system. Experimental data vs model predictions: (○) ter Maat et al.,[22] (△) Huang and Ng,[26] (×) Dicko et al.[30]

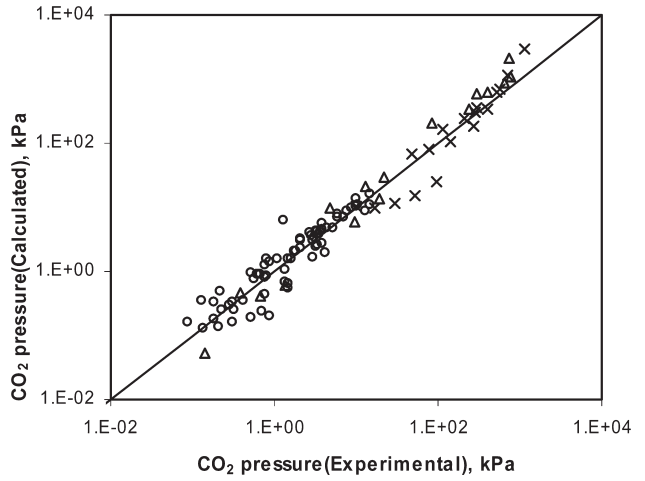

Figure 6. Parity plot for CO_2 partial pressure of $H_2S-CO_2-H_2O-$MDEA system. Experimental data vs model predictions: (○) ter Maat et al.,[22] (△) Huang and Ng,[26] (×) Dicko et al.[30]

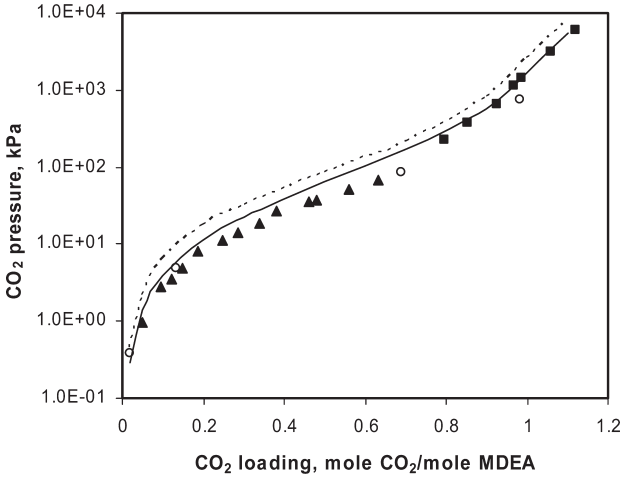

Figure 7. Comparison of the experimental data (symbols) and the model results (lines) for CO_2 partial pressure in aqueous MDEA solution. MDEA mole fraction is 0.13, T = 313 K. (▲) CO_2 pressure data of the CO_2-H_2O-MDEA system from Ermatchkov et al.,[33] (■) CO_2 pressure data of the CO_2-H_2O-MDEA system from Pèrez-Salado Kamps et al.,[28] (○) CO_2 pressure data of the $H_2S-CO_2-H_2O-$MDEA system from Huang and Ng,[26] H_2S loading is fixed to 0.04, (solid line) predicted CO_2 pressure of the ternary CO_2-H_2O-MDEA system, (dotted line) predicted CO_2 pressure of the quaternary $H_2S-CO_2-H_2O-$MDEA system, H_2S loading is fixed to 0.04.

T14 binary. Table 14 shows the correlation results. The average relative deviations on H_2S partial pressures for the three data sets are less than 32%. The regressed NRTL parameters are given in Table 12. Note that these NRTL parameters are assumed to be temperature-independent. Furthermore, the Henry's constant of H_2S in MDEA is set to be same as that of H_2S in water. Figure 3 shows the comparison between the model results and the experimental data for H_2S partial pressures at MDEA mole fractions of 0.13. The model results at other MDEA concentrations are similar. It is evident from Table 14 and Figure 3 that the experimental data are fitted well across all temperatures, pressures, MDEA concentrations, and H_2S loadings. To highlight the results especially at extreme H_2S loadings, Figure3 panels a and b are shown in linear scale in H_2S loading and logarithmic scale in H_2S loading, respectively.

Table 15 shows the comparison between the model predictions and the experimental VLE data from sources not included in the regression. The results highlight the fact that we cannot match all the VLE data because the experimental data from different sources can be inconsistent. For example, the model

dx.doi.org/10.1021/ie102150h |*Ind. Eng. Chem. Res.* XXXX, XXX, 000–000

predictions deviate by almost 65% against the H_2S partial pressure data from Macgregor and Mather (1991).[23] It is also interesting that, although no total pressure data are used in the regression, the model predictions match very well with the three total pressure measurements of Kuranov et al. (1996),[18] Pèrez-Salado Kamps et al. (2001),[28] and Sidi-Boumedine et al. (2004).[29] The average relative deviations on these three total pressure data sets are merely 9.4%, 12.4%, and 12.1%, respectively.

Figure 4 shows that the predicted differential heats of H_2S absorption are compared favorably to the experimental data of Oscarson and Izatt (1990)[31] at MDEA mole fraction of 0.13.

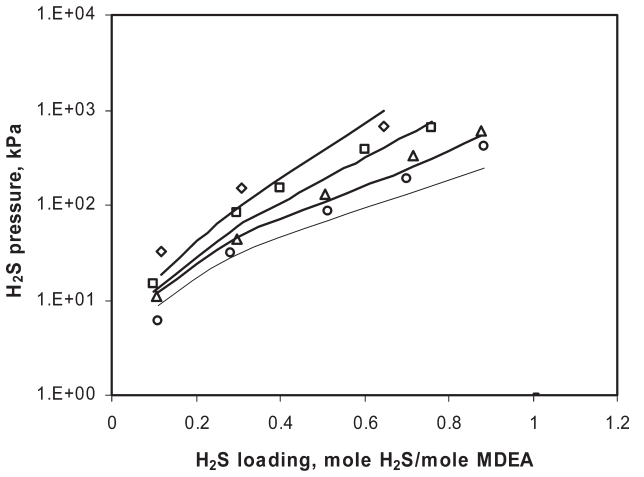

Figure 8. Comparison of the experimental data from Dicko et al.[30] (symbols) and the model results (lines) for H_2S partial pressure of $H_2S-CO_2-H_2O-$MDEA solution. MDEA mole fraction is 0.13, T = 323 K: (○) CO_2 loading is 0.1, (△) CO_2 loading is 0.3, (□) CO_2 loading is 0.5, (◇) CO_2 loading is 0.8.

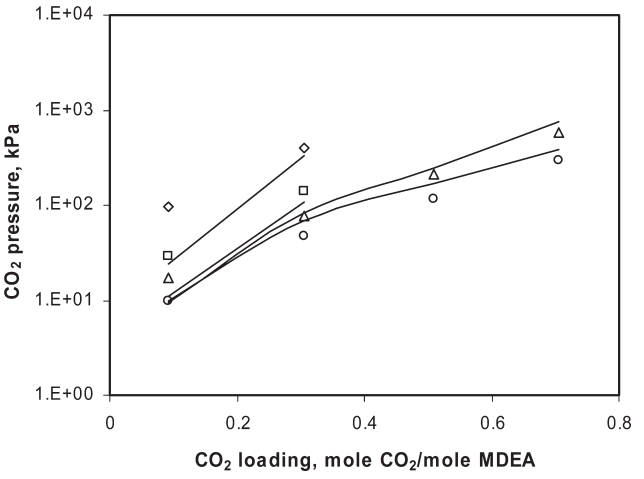

Figure 9. Comparison of the experimental data from Dicko et al.[30] (symbols) and the model results (lines) for CO_2 partial pressure of $H_2S-CO_2-H_2O-$MDEA solution. MDEA mole fraction is 0.13, T = 323 K: (○) H_2S loading is 0.1, (△) H_2S loading is 0.3, (□) H_2S loading is 0.5, (◇) H_2S loading is 0.7.

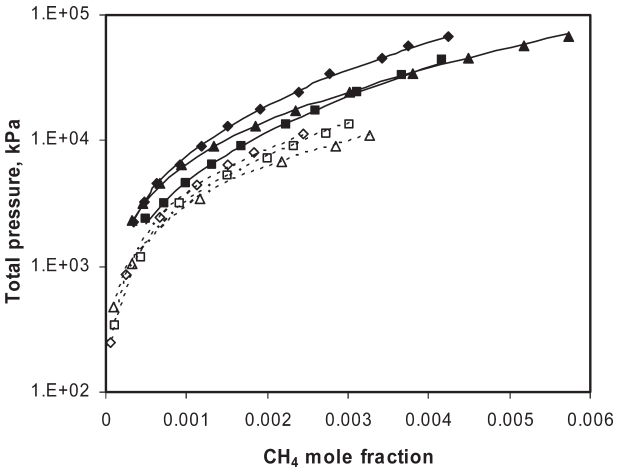

Figure 10. Comparison of the experimental data from Culberson and McKetta[34] (full symbols) and Jou et al.[38] (empty symbols) for CH_4 solubility and the model results (lines); (■) T = 298, (◆) T = 344, (▲) T = 410, (□) T = 298, (◇) T = 343, (△) T = 403 K; (solid line) predicted total pressure of the CH_4-H_2O solution; (dotted line) predicted total pressure of the CH_4-H_2O-MDEA solution.

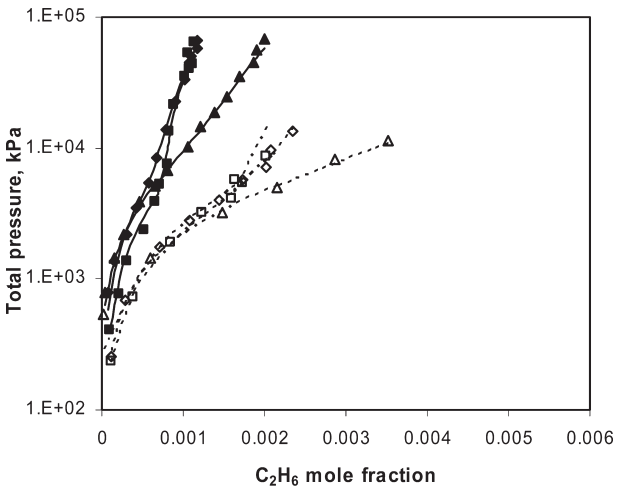

Figure 11. Comparison of the experimental data from Culberson and McKetta[35] (full symbols) and Jou et al.[38] (empty symbols) for C_2H_6 solubility and the model results (lines): (■) T = 311, (◆) T = 344, (▲) T = 411, (□) T = 313, (◇) T = 343, (△) T = 403 K; (solid line) predicted total pressure of the $C_2H_6-H_2O$ solution; (dotted line) predicted total pressure of the $C_2H_6-H_2O-$MDEA solution.

Table 17. Experimental Data Used in the Regression for the Hydrocarbon$-H_2O$ Systems

hydrocarbon	T (K)	P (kPa)	hydrocarbon mole fraction	data points	average relative deviation, $\lvert\Delta P/P\rvert$ (%)	reference
CH_4	298−444	2200−69000	0.00032−0.0078	71	2.9	Culberson and McKetta[34]
C_2H_6	311−444	410−69000	0.000048−0.0032	71	9.8	Culberson and McKetta[35]
C_3H_8	293−368	400−3900	0.000032−0.00026	44	3.8	Chapoy et al.[36]
C_4H_{10}	311−411	135−3400	0.000016−0.00018	63	8.9	Le Breton and McKetta[37]

dx.doi.org/10.1021/ie102150h |*Ind. Eng. Chem. Res.* XXXX, XXX, 000–000

Note that no data on heat of H_2S absorption are included in the regression of the model parameters.

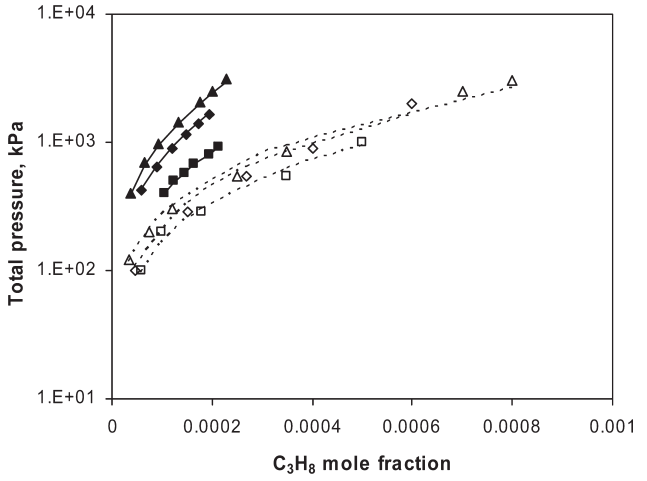

Figure 12. Comparison of the experimental data from Chapoy et al.[36] (full symbols) and Carroll et al.[39] (empty symbols) for C_3H_8 solubility and the model results (lines): (■) T = 298, (◆) T = 323, (▲) T = 353, (□) T = 298, (◇) T = 323, (△) T = 348 K; (solid lines) predicted total pressure of the $C_3H_8-H_2O$ solution; (dashed lines) predicted total pressure of the $C_3H_8-H_2O-$MDEA solution.

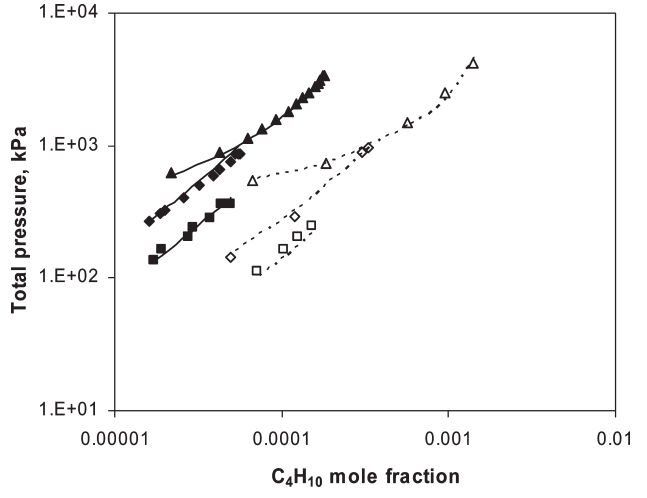

Figure 13. Comparison of the experimental data from Le Breton and McKetta[37] (full symbols) and Jou et al.[40] (empty symbols) for C_4H_{10} solubility and the model results (lines): (■) T = 311, (◆) T = 344, (▲) T = 411, (□) T = 298, (◇) T = 348, (△) T = 423 K; (solid lines) predicted total pressure of the C_4H_{10}-H_2O solution; (dotted lines) predicted total pressure of the $C_4H_{10}-H_2O-$MDEA solution.

The solid lines in Figure 4 are the results determined according to enthalpy balance of the absorption process:

$$\Delta H_{abs} = \frac{n_{final}H^l_{final} - n_{initial}H^l_{initial} - n_{H_2S}H^v_{H_2S}}{n_{H_2S}} \quad (13)$$

ΔH_{abs} is the heat of absorption, H^l_{final} is the molar enthalpy of the final H_2S-H_2O-MDEA solution, $H^l_{initial}$ is the molar enthalpy of the initial H_2S-H_2O-MDEA solution, $H^v_{H_2S}$ is the molar enthalpy of gaseous H_2S absorbed, n_{final}, $n_{initial}$, and n_{H_2S} are the numbers of moles of the final H_2S-H_2O-MDEA solution, the initial H_2S-H_2O-MDEA solution, and the H_2S absorbed, respectively. The differential heat of absorption means the heat effect per unit mole of H_2S when an infinitesimal amount of H_2S is absorbed by the H_2S-H_2O-MDEA solution.

The dashed lines are the differential heats calculated from the Gibbs–Helmholtz equation:[32]

$$\Delta H_{abs} = -RT^2\left[\frac{\partial \ln f_{H_2S}}{\partial T}\right]_{P,x} \quad (14)$$

where f_{H_2S} is the fugacity of H_2S.

The heats calculated from enthalpy balance are differential in loading and constant in temperature, while those calculated from the Gibbs–Helmholtz equation are constant in loading but differential in temperature. Figure 4 shows a very small discrepancy between these two calculations. The discrepancy increases slightly with the increases in temperature and the H_2S loading.

3.3. H_2S-CO_2-H_2O-MDEA System. The available VLE data[22,26,30] for the $H_2S-CO_2-H_2O-$MDEA quaternary system are summarized in Table 16. To properly model the quaternary system, the model requires additional NRTL binary parameters on top of the binary parameters established for the subsystems of H_2S-H_2O-MDEA and CO_2-H_2O-MDEA. Examples are the binary parameters for the H_2S-electrolyte binaries where electrolytes are derived from the ionic reactions between MDEA and CO_2, or the binary parameters for the CO_2-electrolyte binaries where electrolytes are derived from the ionic reactions between MDEA and H_2S. These additional parameters are set to the default values. The acid gas solubility predictions for the $H_2S-CO_2-H_2O-$MDEA quaternary system based on the parameters with the default values are found to be in satisfactory agreement with the experimental data. Figure 5 and 6 show the parity plots for the model predictions versus the experimental data on H_2S and CO_2 partial pressures, respectively. The corresponding relative average deviations between the model predictions and the experimental data for the CO_2 and H_2S partial pressures of the quaternary system are summarized in Table 16. The results show the quality of model predictions for the quaternary system does not degenerate significantly from those for the ternary subsystems. The

Table 18. Experimental Data Used in the Regression for the Hydrocarbon$-H_2O-$MDEA Systems

hydrocarbon	T (K)	P (kPa)	MDEA mole fraction	hydrocarbon mole fraction	data points	average relative deviation, $\lvert\Delta P/P\rvert$ (%)	reference
CH_4	298–403	95–13000	0.0765	0.000042–0.0033	44	6.5	Jou et al.[38]
C_2H_6	298–403	96–13500	0.0765	0.000015–0.0035	45	10.8	Jou et al.[38]
C_3H_8	273–348	100–3000	0.0765	0.000035–0.0008	25	10.3	Carroll et al.[39]
C_4H_{10}	298–423	110–4200	0.0765	0.000049–0.0014	25	11.1	Jou et al.[40]

dx.doi.org/10.1021/ie102150h |Ind. Eng. Chem. Res. XXXX, XXX, 000–000

results also show relatively large discrepancies between the model predictions and the experimental data of Huang and Ng.[26] Figure 7 shows the predicted CO_2 partial pressures of the ternary $CO_2-H_2O-MDEA$ system match the data of Pèrez-Salado Kamps et al. (2001)[28] and Ermatchkov et al. (2006)[33] well. For the quaternary $H_2S-CO_2-H_2O-MDEA$ system, the predicted CO_2 partial pressures increase as H_2S loading increases from 0 to 0.04. However, the CO_2 partial pressures with H_2S loading of 0.04 as reported by Huang and Ng[26] for the quaternary system are much lower than the predictions. In fact, the Huang and Ng data are close to or even lower than the experimental CO_2 partial pressure data reported for the $CO_2-H_2O-MDEA$ ternary system.[28,33] The H_2S partial pressure data of Huang and Ng[26] for the quaternary system show similar behaviors. In addition, Figures 8 and 9 show the comparisons of the model predictions and the experimental data of Dicko et al. (2010)[30] for H_2S and CO_2 partial pressures as one of the CO_2 and H_2S loadings is fixed and the other loading is varied. The model predictions exhibit the trends that H_2S and CO_2 partial pressures increase as the loading of the other solute increases, in line with those of the experimental data.

3.4. Hydrocarbon−H_2O and Hydrocarbon−H_2O−MDEA systems. The Henry's constants for four light hydrocarbons in water are fitted to the total pressure data of the hydrocarbon−water systems. The experimental data[34−37] used in the regression are shown in Table 17. For the CH_4-H_2O and $C_2H_6-H_2O$ systems, the characteristic volume parameters of hydrocarbons and the Henry's constants are regressed together from the gas solubility data with pressure up to 69000 kPa. For the $C_3H_8-H_2O$ and $C_4H_{10}-H_2O$ systems, only the Henry's constants are fitted to the low and mid pressure data up to 3900 kPa. The regressed parameters are summarized in Tables 7 and 10. Figures 10−13 illustrate that the model satisfactorily captures the system nonideality and that the calculated total pressures match the experimental data well. The average relative deviations are less than 10%.

The Henry's constants of the hydrocarbons in MDEA are fitted to the total pressure data of the hydrocarbon−H_2O−MDEA ternary systems. The experimental data[38−40] used in the regression are shown in Table 18. The regressed parameters are given in Table 7. Figures 10−13 show that the calculated total pressures are in good agreement with the experimental data. The average relative deviations are around 10%. Figures 10−13 also show that the hydrocarbon solubilities in the aqueous MDEA solutions increase significantly compared to those in pure water.

4. CONCLUSION

To support process modeling and simulation of the natural gas treating processes with MDEA, the recently developed $CO_2-H_2O-MDEA$ model has been successfully extended to correlate the available experimental solubility data of H_2S and four light hydrocarbons in the aqueous MDEA solutions. The model has been validated for VLE and enthalpy calculations of the $H_2S-H_2O-MDEA$ system with temperature from 283 to 393 K, pressure up to 6000 kPa, MDEA concentration up to 8 m (~50 wt %) and H_2S loading up to 3.2. The model predictions for H_2S and CO_2 partial pressures of the $H_2S-CO_2-H_2O-MDEA$ quaternary system are found to be satisfactory. The model should be a useful tool for accurate calculations of gas solubilities in aqueous MDEA solutions.

AUTHOR INFORMATION

Corresponding Author

*E-mail: chauchyun.chen@aspentech.com. Tel.: 781-221-6420. Fax: 781-221-6410.

ACKNOWLEDGMENT

We thank our colleagues Joe DeVincentis and Yuhua Song for their extensive reviews and helpful comments on this manuscript.

REFERENCES

(1) Zhang, Y.; Chen, C.-C. Thermodynamic Modeling for CO_2 Absorption in Aqueous MDEA Solution with Electrolyte NRTL Model. *Ind. Eng. Chem. Res.* **2011**, *50*, 163–175.

(2) Brelvi, S. W.; O'Connell, J. P. Corresponding States Correlations for Liquid Compressibility and Partial Molar Volumes of Gases at Infinite Dilution in Liquids. *AIChE J.* **1972**, *18*, 1239–1243.

(3) Song, Y.; Chen, C.-C. Symmetric Electrolyte Nonrandom Two-Liquid Activity Coefficient Model. *Ind. Eng. Chem. Res.* **2009**, *48*, 7788–7797.

(4) Chen, C.-C.; Britt, H. I.; Boston, J. F.; Evans, L. B. Local Composition Model for Excess Gibbs Energy of Electrolyte Systems. Part I: Single Solvent, Single Completely Dissociated Electrolyte Systems. *AIChE J.* **1982**, *28*, 588–596.

(5) Gross, J.; Sadowski, G. Perturbed-Chain SAFT: An Equation of State Based on a Perturbation Theory for Chain Molecules. *Ind. Eng. Chem. Res.* **2001**, *40*, 1244–1260.

(6) Gross, J.; Sadowski, G. Application of the Perturbed-Chain SAFT Equation of State to Associating Systems. *Ind. Eng. Chem. Res.* **2002**, *41*, 5510–5515.

(7) *Aspen Physical Property System*, version 7.2; Aspen Technology Inc.: Burlington, MA, 2010.

(8) Wagman, D. D.; Evans, W. H.; Parker, V. B.; Schumm, R. H.; Halow, I.; Bailey, S. M.; Churney, K. L.; Nuttall, R. L. The NBS Tables of Chemical Thermodynamic Properties—Selected Values for Inorganic and C1 and C2 Organic Substances in SI Units. *J. Phys. Chem. Ref. Data* **1982**, *11* (Suppl. No. 2), 1–392.

(9) Criss, C. M.; Cobble, J. W. The Thermodynamic Properties of High Temperature Aqueous Solutions. V. The Calculation of Ionic Heat Capacities up to 200°. Entropies and Heat Capacities above 200°. *J. Am. Chem. Soc.* **1964**, *86*, 5390–5393.

(10) Yan, Y.; Chen, C.-C. Thermodynamic Modeling of CO_2 Solubility in Aqueous Solutions of NaCl and Na_2SO_4. *J. Supercrit. Fluids* **2010**, *55*, 622–633.

(11) Wright, R. H.; Maass, O. The Solubility of Hydrogen Sulphide in Water from the Vapor Pressures of the Solutions. *Can. J. Res. Sect. B.* **1932**, *6*, 91–101.

(12) Phol, H. A. Thermodynamics of the Hydrogen Sulfide-Water System Relevant to the Dual Temperature Process for the Production of Heavy Water. *J. Chem. Eng. Data* **1961**, *6*, 515–521.

(13) Burgess, M. P.; Germann, R. P. Physical Properties of Hydrogen Sulfide−Water Mixtures. *AIChE J.* **1969**, *15*, 272–275.

(14) Clarke, E. C. W.; Glew, D. N. Aqueous Nonelectrolyte Solutions. Part VIII. Deuterium and Hydrogen Sulfides Solubilities in Deuterium Oxide and Water. *Can. J. Chem.* **1971**, *49*, 691–698.

(15) Lee, J. I.; Mather, A. E. Solubility of Hydrogen Sulfide in Water. *Ber. Bunsen-Ges. Phys. Chem.* **1977**, *81*, 1020–1023.

(16) Gillespie, P. C.; Wilson, G. M. Vapor−Liquid Equilibrium Data on Water-Substitute Gas Components: N_2-H_2O, H_2-H_2O, $CO-H_2O$, H_2-CO-H_2O, and H_2S-H_2O. *GPA Research Report RR-41* **1980**, 1–34.

(17) Suleimenov, O. M.; Krupp., R. E. Solubility of Hydrogen Sulfide in Pure Water and in NaCl Solutions, from 20 to 320 °C and at Saturation Pressures. *Geochim. Cosmochim. Acta* **1994**, *58*, 2433–2444.

(18) Kuranov, G.; Rumpf, B.; Smirnova, N. A.; Maurer, G. Solubility of Single Gases Carbon Dioxide and Hydrogen Sulfide in Aqueous

Solutions of *N*-Methyldiethanolamine in the Temperature Range 313−413 K at Pressures up to 5 MPa. *Ind. Eng. Chem. Res.* **1996**, *35*, 1959–1966.

(19) Lemmon, E. W.; Span, R. Short Fundamental Equations of State for 20 Industrial Fluids. *J. Chem. Eng. Data* **2006**, *51*, 785–850.

(20) Jou, F. Y.; Mather, A. E.; Otto, F. D. Solubility of H_2S and CO_2 in Aqueous Methyldiethanolamine Solutions. *Ind. Eng. Chem. Process Des. Dev.* **1982**, *21*, 539–544.

(21) Maddox, R. N.; Bhairi, A. H.; Diers, J. R.; Thomas, P. A. Equilibrium Solubility of Carbon Dioxide or Hydrogen Sulfide in Aqueous Solutions of Monoethanolamine, Diglycolamine, Diethanolamine and Methyldiethanolamine. *GPA Research Report RR-104* **1987**, 1–47.

(22) ter Maat, H.; Praveen, S.; IJben, P.; Arslan, D.; Wouters, H. F.; Huttenhuis, P. J. G.; Hogendoorn, J. A.; Versteeg, G. F. The Determination of VLE Data on CO_2 and H_2S in MDEA and Its Blends with Other Amines. *GPA Research Report RR-186* **2004**, 1–61.

(23) Macgregor, R. J.; Mather, A. E. Equilibrium Solubility of H_2S and CO_2 and Their Mixtures in a Mixed Solvent. *Can. J. Chem. Eng.* **1991**, *69*, 1357–1366.

(24) Jou, F. Y.; Carroll, J. J.; Mather, A. E.; Otto, F. D. The Solubility of Carbon Dioxide and Hydrogen Sulfide in a 25 Weight% Aqueous Solution of Methyldiethanolamine. *Can. J. Chem. Eng.* **1993**, *71*, 264–268.

(25) Li, M. H.; Shen, K. P. Solubility of Hydrogen Sulfide in Aqueous Mixtures of Monoethanolamine with *N*-Methyldiethanolamine. *J. Chem. Eng. Data* **1993**, *38*, 105–108.

(26) Huang, S. H.; Ng, H.−J. Solubility of H_2S and CO_2 in Alkanolamines. *GPA Research Report RR-155* **1998**, 1–31.

(27) Lemoine, B.; Li, Y. G.; Cadours, R.; Bouallou, C.; Richon, D. Partial Vapor Pressure of CO_2 and H_2S over Aqueous Methyldiethanolamine Solutions. *Fluid Phase Equilib.* **2000**, *172*, 261–277.

(28) Pèrez-Salado Kamps, Á.; Balaban, A.; Joedecke, M.; Kuranov, G.; Smirnova, N. A.; Maurer., G. Solubility of Single Gases Carbon Dioxide and Hydrogen Sulfide in Aqueous Solutions of *N*-Methyldiethanolamine at Temperatures from 313 to 393 K and Pressures up to 7.6 MPa: New Experimental Data and Model Extension. *Ind. Eng. Chem. Res.* **2001**, *40*, 696–706.

(29) Sidi-Boumedine, R.; Horstmann, S.; Fischer, K.; Provost, E.; Fuerst, W.; Gmehling, J. Experimental Determination of Hydrogen Sulfide Solubility Data in Aqueous Alkanolamine Solutions. *Fluid Phase Equilib.* **2004**, *218*, 149–155.

(30) Dicko, M.; Coquelet, C.; Jarne, C.; Northrop, S.; Richon, D. Acid Gases Partial Pressures above a 50 wt% Aqueous Methyldiethanolamine Solution: Experimental Work and Modeling. *Fluid Phase Equilib.* **2010**, *289*, 99–109.

(31) Oscarson, J. L.; Izatt, R. M. Enthalpies of Solution of H_2S in Aqueous Methyldiethanolamine Solutions. *GPA Research Report RR-127* **1990**, 1–49.

(32) Kim, I.; Hoff, K. A.; Hessen, E. T.; Haug-Warberg, T.; Svendsen, H. F. Enthalpy of Absorption of CO_2 with Alkanolamine Solutions Predicted from Reaction Equilibrium Constants. *Chem. Eng. Sci.* **2009**, *64*, 2027–2038.

(33) Ermatchkov, V.; Pèrez-Salado Kamps, Á.; Maurer., G. Solubility of Carbon Dioxide in Aqueous Solutions of *N*-Methyldiethanolamine in the Low Gas Loading. *Ind. Eng. Chem. Res.* **2006**, *45*, 6081–6091.

(34) Culberson, O. L.; McKetta, J. J. Phase Equilibria in Hydrocarbon−Water Systems. III—The Solubility of Methane in Water at Pressures to 10000 psia. *Trans. Am. Inst. Min. Metall. Pet. Eng.* **1951**, *192*, 223–226.

(35) Culberson, O. L.; McKetta, J. J. Phase Equilibria in Hydrocarbon−Water Systems. II—The Solubility of Ethane in Water at Pressures to 10000 psi. *Trans. Am. Inst. Min. Metall. Pet. Eng.* **1950**, *189*, 319–322.

(36) Chapoy, A.; Mokraoui, S.; Valtz, A.; Richon, D.; Mohammadi, A. H.; Tohidi, B. Solubility Measurement and Modeling for the System Propane−Water from 277.62 to 368.16 K. *Fluid Phase Equilib.* **2004**, *226*, 213–220.

(37) Le Breton, J. G.; McKetta, J. J. Low Pressure Solubility of *n*-Butane in Water. *Hydrocarbon Process. Pet. Refiner* **1964**, *43*, 136–138.

(38) Jou, F. Y.; Carroll, J. J.; Mather, A. E.; Otto, F. D. Solubility of Methane and Ethane in Aqueous Solutions of Methyldiethanolamine. *J. Chem. Eng. Data* **1998**, *43*, 781–784.

(39) Carroll, J. J.; Jou, F. Y.; Mather, A. E.; Otto, F. D. Phase Equilibria in the System Water−Methyldiethanopropanylamine. *AIChE J.* **1992**, *38*, 511–520.

(40) Jou, F. Y.; Carroll, J. J.; Mather, A. E.; Otto, F. D. Phase Equilibria in the System *n*-Butane−Water−Methyldiethanolamine. *Fluid Phase Equilib.* **1996**, *116*, 407–413.